RSC Advances

PAPER

View Article Online
View Journal | View Issue

Cite this: *RSC Adv.*, 2025, **15**, 41241

The synthesis and study of carboxymethyl cellulose from water hyacinth biomass stabilized silver nanoparticles for a colorimetric detection sensor of Hg(II) ions

Panida Thepwat, Apichart Saenchoopa, Wipada Onnet, Phakamas Namcharee, Chonlatan Sanmanee, Kittiya Plaeyao, Sirinan Kulchat and Suppanat Kosolwattana *

Received 4th July 2025
Accepted 17th October 2025

DOI: 10.1039/d5ra04757a

rsc.li/rsc-advances

This study aims to synthesize silver nanoparticles, using carboxymethyl cellulose from water hyacinth biomass by a direct synthesis method, for the detection of Hg^{2+}, which is a hazardous heavy metal that pollutes the environment. The successful synthesis of carboxymethyl cellulose from water hyacinth biomass to stabilize silver nanoparticles (CMC-AgNPs) was confirmed by UV-vis spectroscopy with a surface plasmon resonance band at 410 nm. CMC-AgNPs were then identified using UV-vis spectroscopy, X-ray diffraction (XRD), Fourier transform infrared spectroscopy (FTIR), transmission electron microscopy (TEM), energy-dispersive X-ray spectroscopy (EDX) and zeta potential, before the study of Hg^{2+} detection. When the CMC-AgNPs solution comes into contact with mercury, a redox reaction occurs between mercury and CMC-AgNPs, resulting in a color change from yellow to colorless. The effects of different parameters, such as CMC-AgNPs concentration, reaction time and pH for detecting Hg^{2+}, were studied, and the limit of detection (LOD) and limit of quantitation (LOQ) in this study were 3.14 μM and 10.45 μM, respectively. Moreover, CMC-AgNPs were used to prepare Hg^{2+} detection films to enhance the convenience of measurement.

1. Introduction

Due to the negative impact of heavy metal pollution on the ecosystem worldwide, the issue is becoming worse and has created serious concerns. The explosive expansion of the metal and agricultural industries, inadequate waste management, and the use of pesticides and fertilizers are all contributing factors to the disposal of these inorganic pollutants in our air, water, and soil. One of the most dangerous and persistent heavy metal contaminants that affect both people and the environment is mercury (Hg^{2+}). The primary routes of human exposure are through consuming contaminated fish and using dental amalgams.[1] Mercury also affects various systems in the human body, such as the cardiovascular system, the central nervous system,[2] the endocrine system[3] and the immune system.[4] Various analytical methods have been developed to detect mercury ions, including electrochemical, biosensors,[5] fluorescence[5] and colorimetric methods.[6] Among these analytical methods, colorimetric sensors are widely recognized for their high sensitivity and ability to respond selectively to different analytes.[7]

The water hyacinth belongs to the Pontederiaceae family of freshwater plants. It is a perennial,[8] free-floating species that grows quickly. It is recognized as one of the most concerning invasive species and a pervasive aquatic weed globally.[9] Furthermore, water hyacinth contributes to issues in agriculture, irrigation and public health. The rapid dispersion of water hyacinth results in the obstruction of rivers and canals, the destruction of native plants, and the degradation of water quality (such as oxygen levels, pH, and temperature), limiting sunlight penetration. Water pollution issues may arise from rapidly spreading aquatic weeds, such as water hyacinth,[10] which cause water to become polluted, leading to the death of aquatic animals. Additionally, it can result from mercury contamination in water sources, which is attributable to industrial activities and the agricultural use of chemical fertilizers.[11,14] These issues significantly affect human health and the environment,[12] and require timely action to prevent negative impacts. Nevertheless, water hyacinth is a valuable biomass source for bioenergy production. The plant contains up to 25% cellulose, 33% hemicellulose, and 10% lignin, making it suitable as a feedstock to produce cellulose-based polymers.[13] To enhance the hydrophilic properties of cellulose, it can be modified into cellulose derivatives, such as carboxymethyl cellulose (CMC). CMC is a cellulose-based compound that

Department of Chemistry, Khon Kaen University, Khon Kaen, 40002, Thailand. E-mail: suppako@kku.ac.th

contains carboxymethyl functional groups.[14] The synthesis of CMC is carried out through a two-step process.[15] The first step is alkalization, using NaOH and an organic solvent to activate the functional groups of cellulose. The second step is esterification, where the –OH groups of cellulose react with monochloroacetic acid, resulting in the formation of CMC.[15] The functional group of CMC enhances its water solubility;[16] CMC also serves as an effective dispersant and stabilizing agent in colloidal systems, such as in the synthesis of nanoparticles. Due to its large molecular structure and negatively charged groups, CMC helps prevent the aggregation of silver nanoparticles by providing electrostatic repulsion and steric stabilization.[17,18]

Silver nanoparticles (AgNPs) are being increasingly applied in a wide range of fields, including pharmaceuticals, food safety, public health, bio-medical engineering, bio-sensing, and industry, owing to their distinctive physical and chemical characteristics.[19–21] AgNPs are widely applied as colorimetric sensors to detect ions of various heavy metals, such as copper(II),[22] lead(II),[22] cadmium(II)[23] and mercury(II),[24] and can be synthesized using various methods, such as chemical, physical and biological methods. Biogenic synthesis of nanoparticles is recognized as a green chemistry approach, utilizing plant-based materials,[25] edible substances,[26] algae[27] and herbal products.[28] These extracts are used as stabilizing agents in addition to reducing agents for the fabrication of silver nanoparticles.[29]

This study proposed the synthesis of cellulose and CMC from water hyacinth biomass. The CMC was then used to stabilize silver nanoparticles (CMC-AgNPs), as CMC possesses both reducing and stabilizing properties.[30] These CMC-AgNPs were employed in a colorimetric sensor to detect Hg^{2+} through redox reactions between Hg^{2+} and CMC-AgNPs. The sensor is designed as a colorimetric sensor in both solution and film for Hg^{2+} detection. Furthermore, it enhances the benefits of water hyacinth by functioning as a material for developing sensor films and being utilized in synthesizing Hg^{2+} detection sensors (Scheme 1).

2. Materials and methods

2.1 Materials

The water hyacinths were taken from a lake in Thailand. Sodium hydroxide (NaOH, RCI Labscan), sodium chlorite ($NaClO_2$, DC Fine Chemicals SLU), sodium chloroacetate (Sigma-Aldrich, Germany), silver nitrate ($AgNO_3$, POCH™), sodium nitrate ($NaNO_3$, Univar, Australia), magnesium nitrate ($Mg(NO_3)_2$, Univar, Australia), barium nitrate ($Ba(NO_3)_2$, Univar, Australia) and cobalt(II)nitrate hexahydrate($Co(NO_3)_2 \cdot 6H_2O$, Univar, Australia), manganese(II)nitrate tetrahydrate ($Mn(NO_3)_2 \cdot 4H_2O$, Sigma Aldrich, China), lead(II)nitrate ($Pb(NO_3)_2$, Carlo Erba), nickel(II)nitrate hexahydrate ($Ni(NO_3)_2 \cdot 6H_2O$, Carlo Erba), and cadmium nitrate tetrahydrate ($Cd(NO_3)_2 \cdot 4H_2O$, Carlo Erba), potassium nitrate (K_2NO_3, BDH, England), calcium chloride ($CaCl_2$, Scharlau, Spain), copper(II) nitrate trihydrate ($Cu(NO_3)_2 \cdot 3H_2O$, Fluka, Switzerland), zinc nitrate hexahydrate ($Zn(NO_3)_2 \cdot 6H_2O$, Fluka, Switzerland), chromium chloride hexahydrate ($CrCl_3 \cdot 6H_2O$, BDH, England), dipotassium phosphate (K_2HPO_4, QRec™), potassium dihydrogen phosphate (KH_2PO_4, QRec™), and mercury(II) chloride ($HgCl_2$, QRec™). Hydrochloric acid (37%), methanol, and isopropanol were purchased from RCI Labscan, Thailand. Deionized water (DI) with specific resistivity of 18.2 MU cm was obtained from a RiOs™ TypeI Simplicity 185 (millipore water purification system), antimicrobial activity assays used *Escherichia coli* ATCC 25922 and *Staphylococcus aureus* ATCC 25923.

2.2 Extraction of cellulose from water hyacinth

The dried water hyacinth was ground into a fine powder and dissolved in 4% NaOH at room temperature for 4 hours. The mixture was washed 3 times with distilled water, filtered, and dried at 60 °C overnight. The dried fibrous material was then treated with 1 M HCl and stirred at 80 ± 5 °C for 3 hours. After cooling naturally to room temperature, the brown residue was washed with distilled water until neutral, filtered using a vacuum pump, and dried at 60 °C overnight. For the alkaline treatment, the water hyacinth fiber was directly treated with 2% NaOH at approximately 80 °C for 2 hours under continuous stirring. The sample was then filtered using filter paper in a Buchner funnel with a vacuum pump and left to dry at room temperature. In the final step, the fibers underwent bleaching by mixing with 4% sodium chlorite ($NaClO_2$) and heating at 60 °C under constant stirring. The resulting cellulose was filtered using a vacuum pump and dried at room temperature.

2.3 Synthesis of carboxymethyl cellulose from water hyacinth

About 10 g cellulose, 80 mL isopropanol (IPA) and 20 mL 30% NaOH were mixed and stirred at 60 °C for 1 h. After 1 h, 3 g of sodium chloroacetate was added to the mixture, and the solution was stirred continuously for 3 hours at 60 °C. The fiber was filtered with a vacuum pump and then washed with 100 mL methanol and neutralized using 1% acetic acid. The mixture was soaked overnight at room temperature. The CMC product obtained was washed with methanol 2 times before being filtered and dried at ambient temperature.

2.4 Synthesis of CMC-AgNPs

Carboxymethyl cellulose was mixed into 50 cm^3 of distilled water until fully dissolved. The pH of the solution was adjusted to 12. Subsequently, the temperature of the reaction was elevated to 70 degrees celsius. Then, 1 cm^3 of silver nitrate solution 0.1 N was added drop by drop. The reaction mixture was subjected to continuous stirring for 1 h. After that, the solution was cooled down at room temperature and purified by centrifugation at 8000 rpm for 20 min and the resulting solution filtered using a nylon syringe filter (diameter 25 mm, pore size 0.22 mm). The solution immediately turned yellow-brown after the addition of silver nitrate, indicating the formation of silver nanoparticles, which was confirmed by UV-vis absorption spectroscopy.

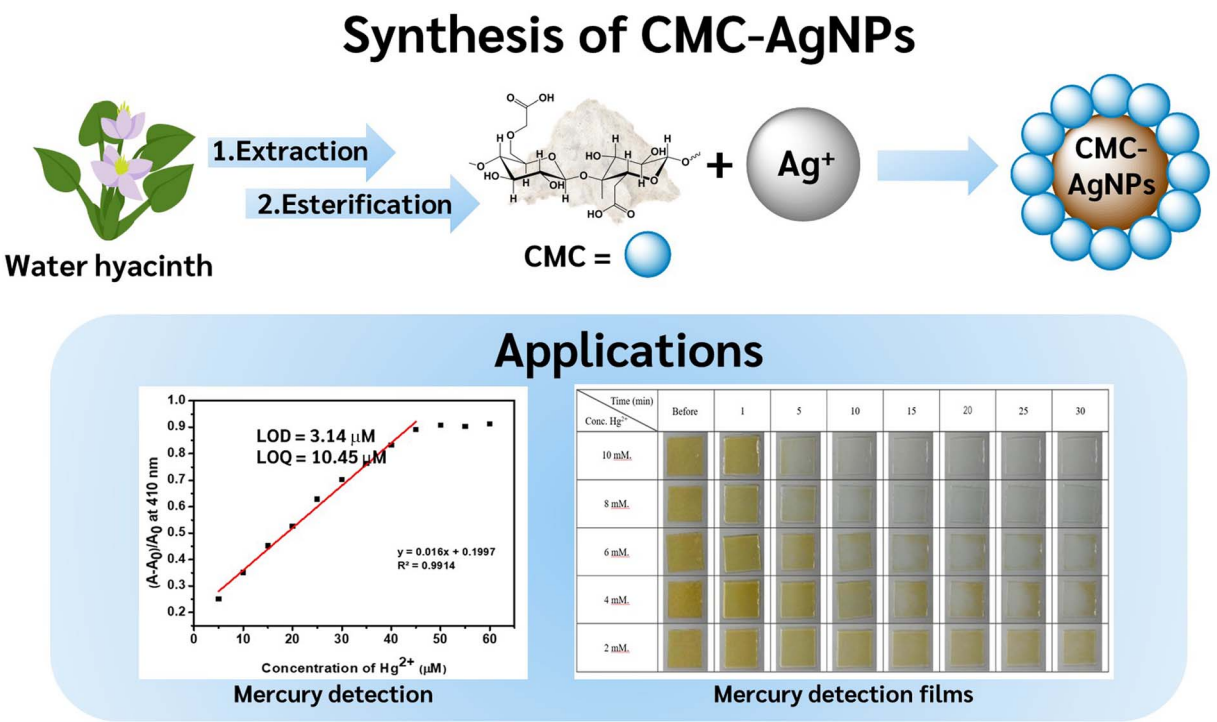

Scheme 1 A schematic illustration of CMC-AgNPs from water hyacinth and their applications in mercury detection and as an anti-bacterial.

2.5 Calculation of concentration of silver nanoparticles

To calculate the concentration of silver nanoparticles in this study, the following equations[34] were used. Initially, the average number of atoms per nanoparticle (N) was determined using eqn (1):

$$N = \frac{\pi \rho D^3}{6M} N_A \quad (1)$$

where ρ is the density of face-centered, cubic (fcc) silver (10.5 g cm^{-3}), D is the average diameter of nanoparticles (=13.3 nm as determined by TEM), M is the atomic mass of silver, and N_A is Avogadro's number. If all the silver ions in the initial solution were converted into silver nanoparticles ($N = 82\,407$), the molar concentration of silver nanoparticles (C) in the solution is then estimated to be approximately eqn (2):

$$C = \frac{N_T}{NVN_A} \quad (2)$$

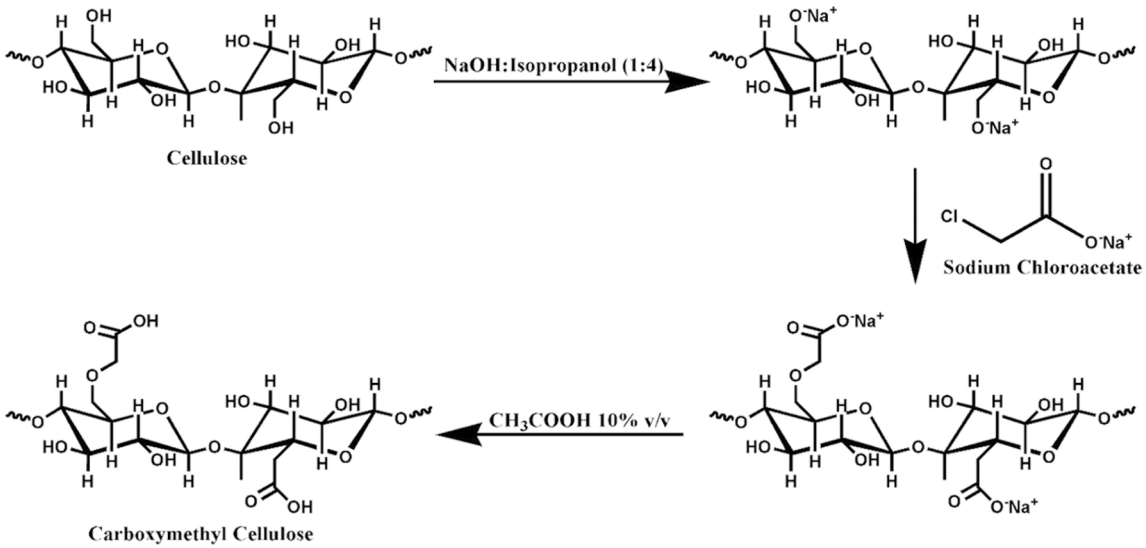

Fig. 1 Schematic of the synthesis of carboxymethyl cellulose.

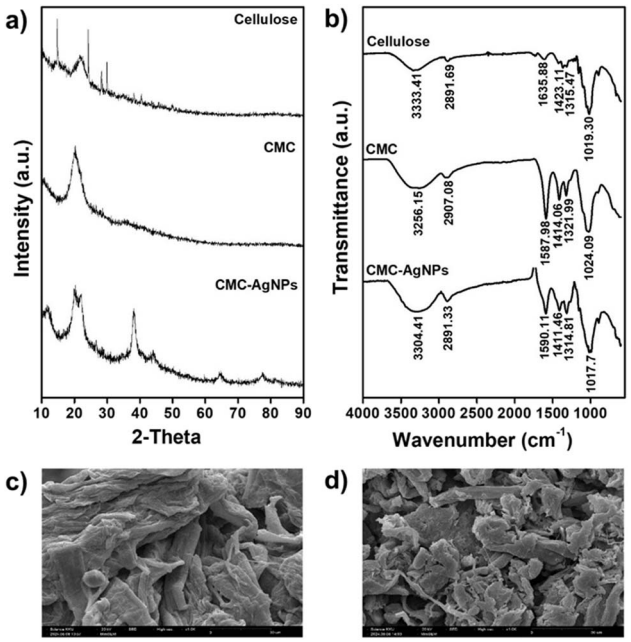

Fig. 2 XRD pattern (a) and ATR-FTIR spectra (b) of cellulose from water hyacinth, CMC, CMC-AgNPs. SEM image (c) of cellulose and SEM image (d) of CMC.

where N_T is the number of silver atoms added as $AgNO_3$ (0.001 mol), N is the atoms per nanoparticle (from eqn (1)), and V is the solution volume (0.051 L), giving the concentration of CMC-AgNPs as 23.3 nM.

2.6 Characterization of silver nanoparticles

The creation of CMC-AgNPs was proved by Bruker's X-ray Diffractometer (Model: D8 Advance). The absorption spectrum of AgNPs was measured with a UV-vis spectrophotometer (Agilent Technologies Cary 60, Germany). The morphology and size of silver nanoparticles were imaged by the Tecnai G2-20 transmission electron microscope (TEM) at an acceleration voltage of 200 kV (FEI, Netherlands). The confirmation of functional groups on the silver nanoparticle's surface was evaluated using Bruker TENSOR 27. Attenuated total reflection Fourier transform infrared spectra (ATR-FTIR) in the range of 4000 to 600 cm^{-1} wavelengths were obtained. Inductively coupled plasma optical emission spectroscopy (ICP-OES) determined the total Ag of silver nanoparticle solution. The zeta potential of CMC-AgNPs was measured using a Malvern instrument zetasizer nano ZS (UK). The surface chemical properties of CMC-AgNPs was characterized using X-ray photoelectron spectroscopy (XPS).

2.7 Colorimetric sensing of Hg^{2+} by UV-vis spectroscopy

The ability of AgNPs to detect Hg^{2+} ions was tested by adding 100 μL of CMC-AgNPs solution to a 5 mL volumetric flask. Then, deionized water and 0.1 M Tris–HCl buffer solution (pH 3) 1 mL were added, followed by 15 μL of 10 mM mercury solution, and the solution was adjusted to a final volume. Other metal ions (Na^+, K^+, Ca^{2+}, Mg^{2+}, Ba^{2+}, Mn^{2+}, Pb^{2+}, Ni^{2+}, Cu^{2+}, Cd^{2+}, Cr^{2+}, Zn^{2+}, and Co^{2+}) were also similarly tested by the same method. Finally, UV-vis spectra using UV-vis spectroscopy were used to examine the sensitivity of CMC-AgNPs for mercury in comparison to other heavy metals under the same conditions. All tests were performed at room temperature and repeated three times.

2.8 Naked-eye detection of Hg^{2+} in water

For the naked-eye detection of metal ions, 100 μL of a 23.3 nM CMC-AgNPs solution was added into a 5 mL volumetric flask. 1 mL of 0.1 M Tris–HCl buffer (pH 3.0) and 50 μL of a 10 mM metal ion solution were added. The final volume was adjusted to 5 mL with DI water. To evaluate the sensitivity for naked-eye detection of Hg^{2+}, varying volumes of a 10 mM Hg^{2+} stock solution were added to the CMC-AgNPs and Tris–HCl buffer mixture, resulting in final Hg^{2+} concentrations of 5, 10, 15, 20, 40, and 100 μM.

2.9 Preparation of composite films for Hg^{2+} ion detection

The composite films for Hg^{2+} ion detection were prepared by dissolving 6 g of polyvinyl alcohol (PVA) in 100 mL of deionized water and incorporating 4 mL of glycerol as a plasticizer. Separately, we dissolved 0.7 g of cassava starch in 100 mL of deionized water, heated and stirred at 60 °C, then added 4 mL of glycerol. Once the PVA and starch solutions were fully dissolved, we combined them and stirred them at 80 °C for 1 hour. After the solution has cooled, we added 10 mL of CMC-AgNPs and 20 mL of pH 3 buffer. The resulting solution was then cast onto a plate and dried at 60 °C to form a film.

3. Results and discussion

3.1 Characterization of carboxymethyl cellulose from water hyacinth

The cellulose extraction from water hyacinth begins with immersing the water hyacinth in a sodium hydroxide solution, which induces swelling of the plant tissue. The alkaline solution penetrates the amorphous regions of the plant cell wall structure, resulting in the breakdown of molecular bonds due to the stress generated. After the alkaline treatment, the hydrolysis of water hyacinth fibers with hydrochloric acid breaks down the hemicellulose structure associated with cellulose, leading to its removal. This process results in the remaining structure consisting of lignin and cellulose, which is degraded into smaller fragments. Subsequently, alkaline treatment is employed to separate lignin from cellulose. Due to the solubility of lignin in alkaline conditions, a dark brown solution of lignin is obtained in this step, while cellulose remains a white, insoluble solid. The bleaching process using a 2% w/v NaOH solution effectively removes residual lignin and hemicellulose; this process also increases the whiteness of the cellulose fibers.[13]

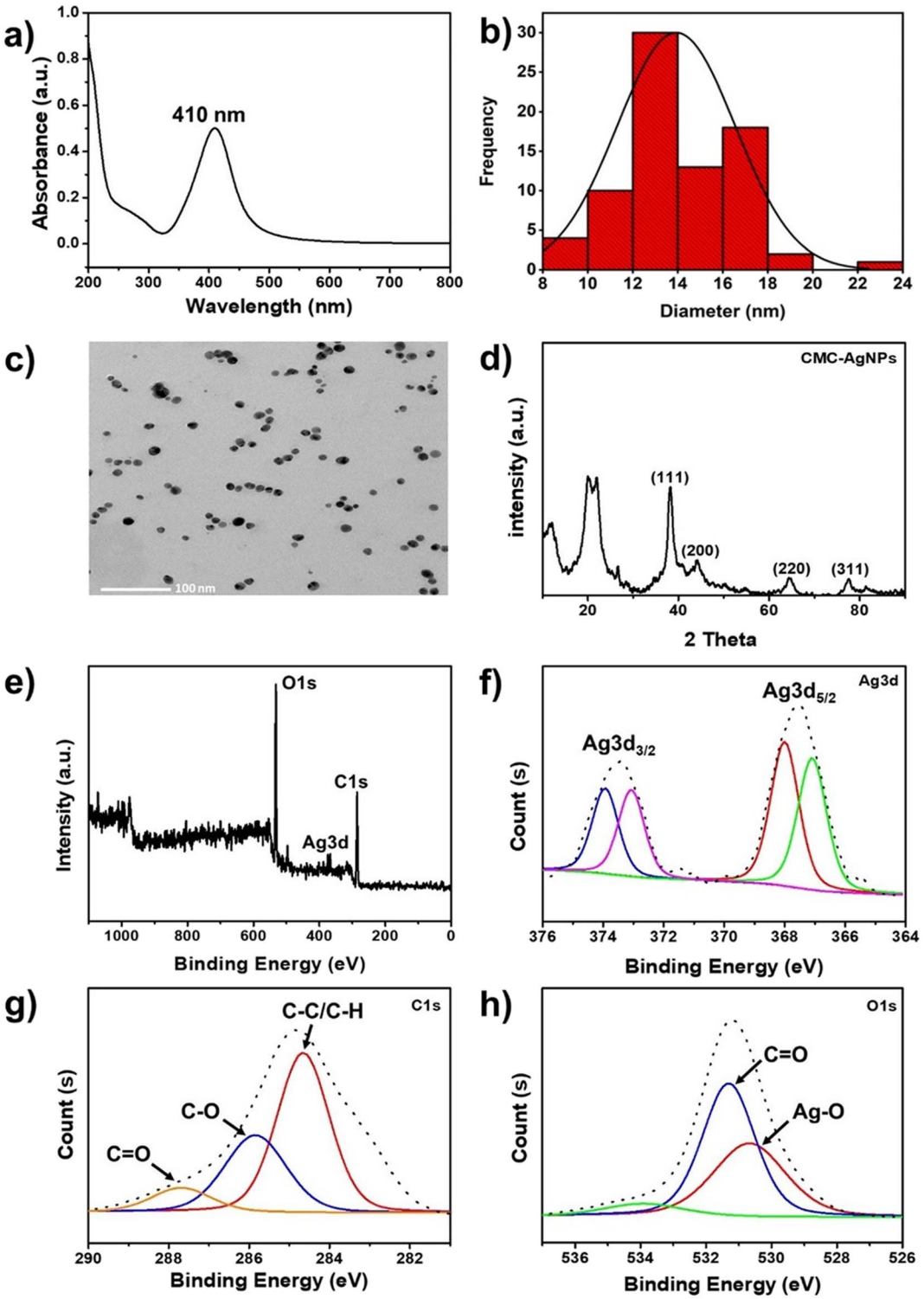

Fig. 3 UV-vis absorption spectra (a) of CMC-AgNPs, size distribution plot (b) of CMC-AgNPs from TEM, TEM image (c) of CMC-AgNPs, XRD pattern (d) of CMC-AgNPs, XPS spectra (e–h) of CMC-AgNPs.

3.2 Synthesis of carboxymethyl cellulose from water hyacinth

The synthesis process of carboxymethyl cellulose is shown in Fig. 1. A solution of 30% sodium hydroxide and isopropanol was added, resulting in the exchange at the hydroxyl group at carbon position 6 in the cellulose structure, where sodium ions substitute hydride ions. The addition of sodium chloroacetate results in the substitution of sodium ions with carboxymethyl groups (CH_3COONa^+). A methanol solution is employed to remove any unreacted groups not involved in the

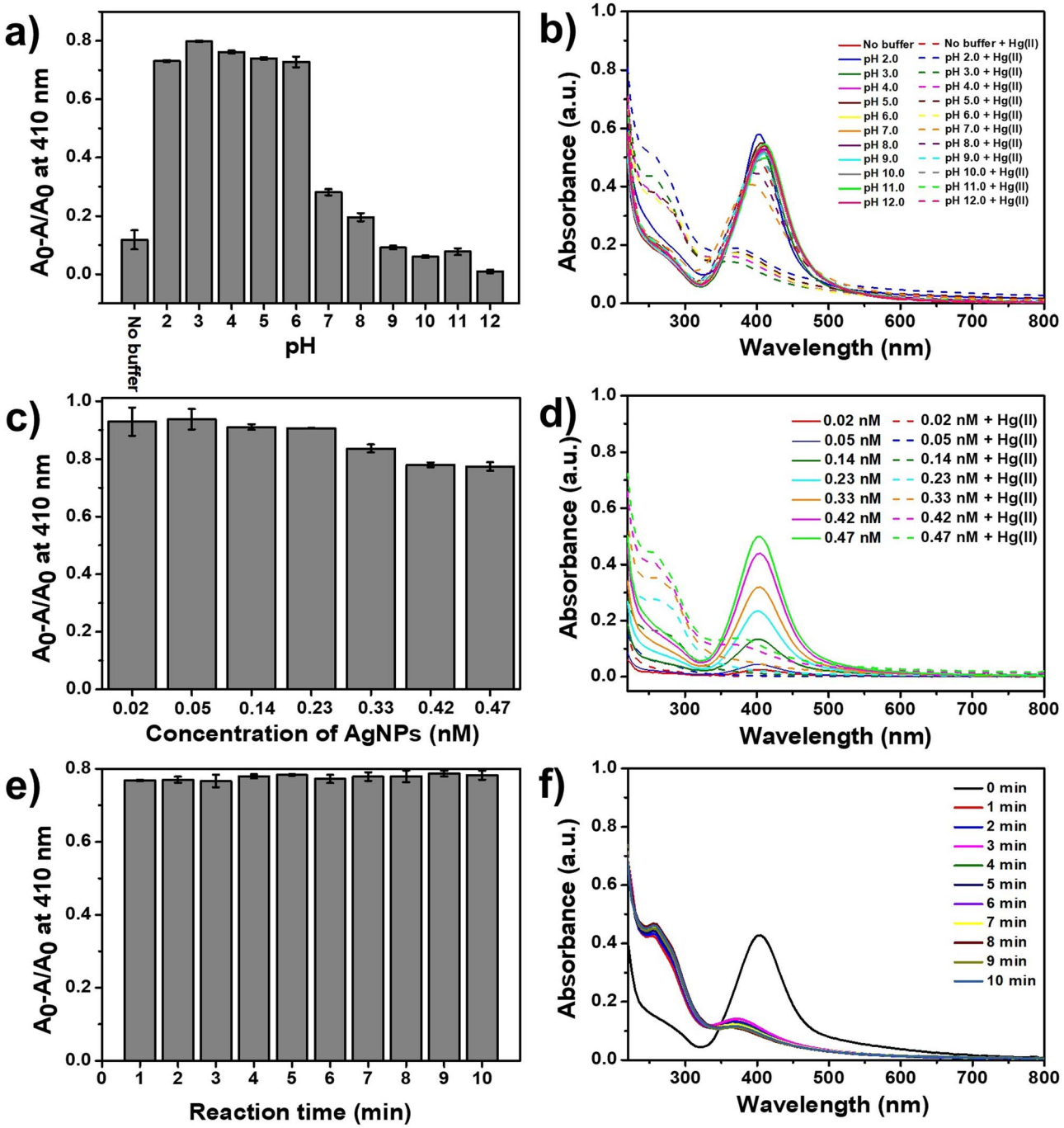

Fig. 4 Relative change in the absorbance (a) of CMC-AgNPs in the presence of Hg^{2+} (30 μM) and 0.1 M of buffer solution at different pH from 2.0 to 12.0, the corresponding UV-vis absorption spectra (b) for the data in panel (a), relative change in the absorbance (c) of CMC-AgNPs as a function of CMC-AgNPs volume in the presence of Hg^{2+} (30 μM) and 0.1 M of Tris–HCl buffer solution at pH 3.0, the corresponding UV-vis absorption spectra (d) for the data in panel (c), relative change (e) of the absorbance of CMC-AgNPs as a function of time in the presence of Hg^{2+} (30 μM) and 0.1 M of HOAc buffer solution at pH 3.0, the corresponding UV-vis absorption spectra (f) for the data in panel (e).

formation of carboxymethyl cellulose, and acetic acid subsequently mediates an ion exchange between sodium ions and hydride ions, leading to the incorporation of carboxymethyl groups into the cellulose structure.[31]

3.3 Characterization of cellulose and carboxymethyl cellulose

The X-ray diffraction (XRD) technique analyzes naturally occurring polymer crystallinity degree and structural characteristics as shown in Fig. 2(a). The diffraction patterns show a reduced crystallinity in CMC compared to cellulose. The

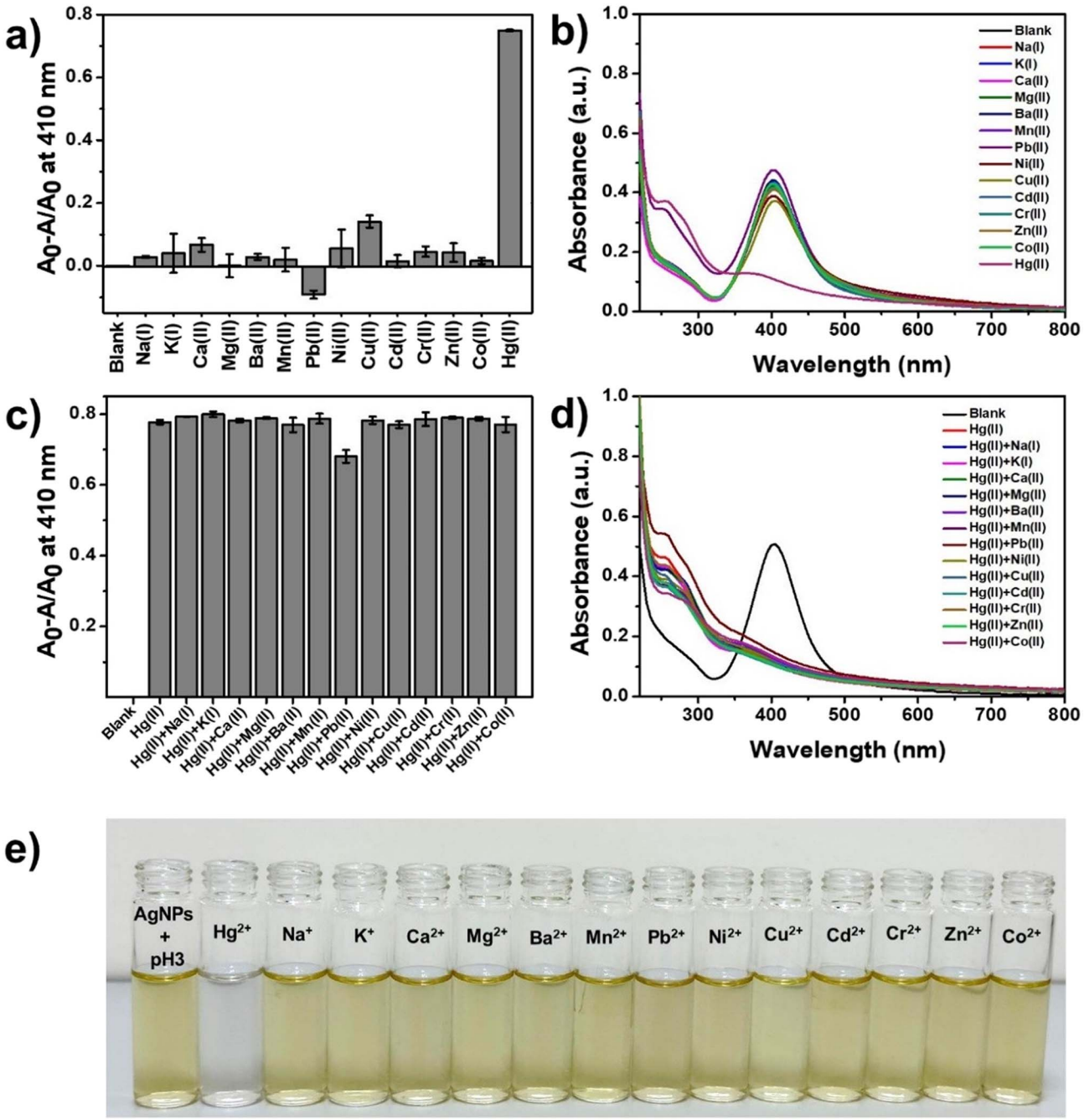

Fig. 5 Relative change (a) of the absorbance of CMC-AgNPs in the presence of 30 μM Hg^{2+} and various metal ions in 0.1 M HOAc buffer solution at pH 3.0, (b) the UV-vis absorption spectra (a) for the data in panel. Relative change (c) of the absorbance of CMC-AgNPs in the presence of 30 μM Hg^{2+} and 100 mM of various metal ions in 0.1 M HOAc buffer solution at pH 3.0, the UV-vis absorption spectra (d) for the data in panel (c), photograph (e) of the colorimetric response of CMC-AgNPs in the presence of 30 μM of various metal ions in 0.1 M HOAc buffer solution at pH 3.0.

synthesis of CMC from cellulose results in structural modifications due to the incorporation of methyl groups. Therefore, it can be inferred that the synthesized CMC demonstrates improved water solubility, due to the increased amorphous phase of the structure.[32] The functional groups of the synthesized CMC were confirmed by Fourier transform infrared spectroscopy (FT-IR). The spectrum of cellulose is shown in Fig. 2(b), the broad band of O–H stretching at 3333 cm^{-1}, C–H stretching at 2891 cm^{-1}, and bound H_2O stretching at 1635 cm^{-1}. The bands around 1423 and 1315 cm^{-1} are assigned to $-CH_2$ scissoring and –OH bending vibration respectively. The peak at 1019 cm^{-1} is assigned to C–O–C bending.[33] The FT-IR spectrum of carboxymethyl cellulose shows absorption bands at 3256 cm^{-1} and 2907 cm^{-1}, which are assigned to O–H stretching and C–H stretching respectively. The absorption band at 1587 cm^{-1} confirmed the C=O group stretching of

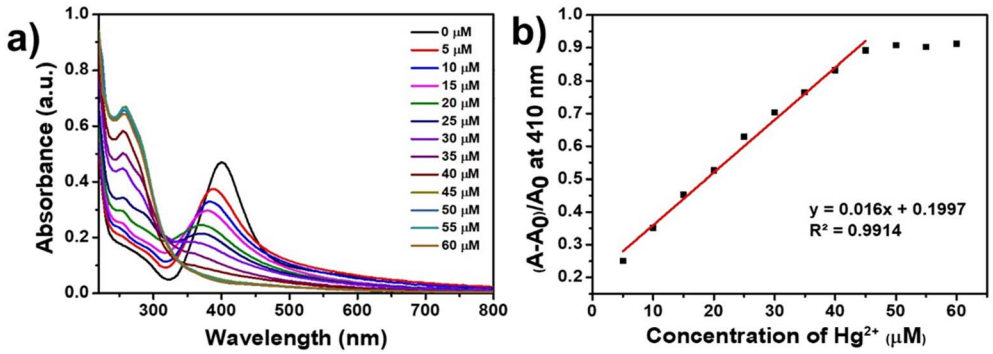

Fig. 6 The UV-vis absorption spectra (a) of CMC-AgNPs after treatment with different concentrations of Hg^{2+} from 5 to 60 μM in 0.1 M buffer solution at pH 3.0. The absorbance ratio $(A - A_0)/A_0$ at 410 nm (b) is a function of Hg^{2+} concentration.

carboxymethyl.[33] The microstructures of cellulose and CMC were analyzed using SEM and are presented in Fig. 2(c) and (d). Cellulose exhibits a disordered fibrous morphology, which results from the bleaching process, which causes fiber fragmentation and separation. CMC exhibits an irregular morphology[34] with non-uniform particle sizes, formation with visible cracks or wrinkles, and a rough surface,[35] which is attributed to the presence of carboxyl groups attached to the cellulose surface.

3.4 Characterization of CMC-AgNPs

CMC-AgNPs were successfully prepared using the green synthesis method, where CMC is a polymer with –COOH functional groups that can react with silver ions (Ag^+). In this process, CMC acts as a reducing agent, helping to reduce Ag^+ ions into nano-sized silver nanoparticles (Ag^0). Additionally, CMC also functions as a stabilizing agent by preventing the aggregation of AgNPs due to the –COOH groups, which help to bind and maintain the small size and good dispersion of the silver nanoparticles.[30] The formation of AgNPs was verified using UV-vis spectroscopy, which showed a surface plasmon resonance peak at 410 nm (Fig. 3(a)). The size and morphology of synthesized silver nanoparticles were demonstrated by transmission electron microscopy (TEM) showing that the particle size was 13.9 ± 2.6 nm, calculated using the ImageJ program with a spherical shape and uniform distribution (Fig. 3(b) and (c)). Elemental analysis was performed using EDX spectroscopy (Fig. S1). The results validated the detection of silver in the EDX spectra, confirming the production of silver nanoparticles. The carbon and oxygen elements detected are components of CMC. The peak of Cu observed corresponds to the use of copper grids as sample holders. The X-ray diffraction pattern of the AgNPs showed the diffraction peaks at 2θ values of 38.27°, 44.11°, 64.39° and 77.71°, which correspond to the (111), (200), (220) and (311) lattice planes, respectively. These diffraction peaks correspond with the joint committee on powder diffraction standards (JCPDS) profile for the face-centered cubic (fcc) structure of silver (Fig. 3(d)). The broad peak around 2θ values ranging from 15° to 30° corresponds to the disordered structure of CMC. The FT-IR spectrum (Fig. 2(a)) revealed the functional group CMC-AgNPs compared to CMC. The spectrum band at 3304 cm^{-1} is assigned to O–H stretching, proving that hydroxyl groups are attached to the surface of the silver nanoparticle. The peaks at 2891 cm^{-1} and 1590 cm^{-1} were assigned to C–H stretching and C=O stretching of carboxymethyl. The results suggest that CMC particles are present on the surface of the silver nanoparticles. The XPS spectra (Fig. 3(e)) show the spectrum survey of CMC-AgNPs reveals the presence of elements C, O and Ag. The Ag3d spectrum (Fig. 3(f)) consists of $Ag3d_{3/2}$ and $Ag3d_{5/2}$.These peaks confirm the presence of silver in the sample. The binding energy (BE) values indicate the metallic (Ag^0) form of silver. Since CMC acts as a stabilizing and reducing agent, oxygen (O 1s) and carbon (C 1s) peaks will be present due to the carboxyl (–COO–) and hydroxyl (–OH) groups.[36] In the C 1s spectrum (Fig. 3(g)), different chemical states of carbon in CMC are reflected, including C–C/C–H, C–O, and O–C=O.[37,38] In the O 1s spectrum (Fig. 3(h)), peaks corresponding to C=O from CMC and Ag–O bonding indicate the interaction between AgNPs and oxygen-containing functional groups from CMC. The presence of these peaks confirms that CMC is interacting with AgNPs. Additionally, the presence of CMC-AgNPs was confirmed by inductively coupled plasma optical emission spectroscopy (ICP-OES), which showed an Ag concentration of 3.18 mg L^{-1}.

Table 1 Determination of Hg^{2+} concentrations in a real water sample

		Proposed method ($n = 3$)		
Water sample	Added Hg^{2+} (μM)	Found Hg^{2+} (μM)	% Recovery ± SD	RSD (%)
Tap water	10	9.90 ± 0.26	99.01 ± 2.56	2.58
	20	20.13 ± 0.33	100.65 ± 1.65	1.64

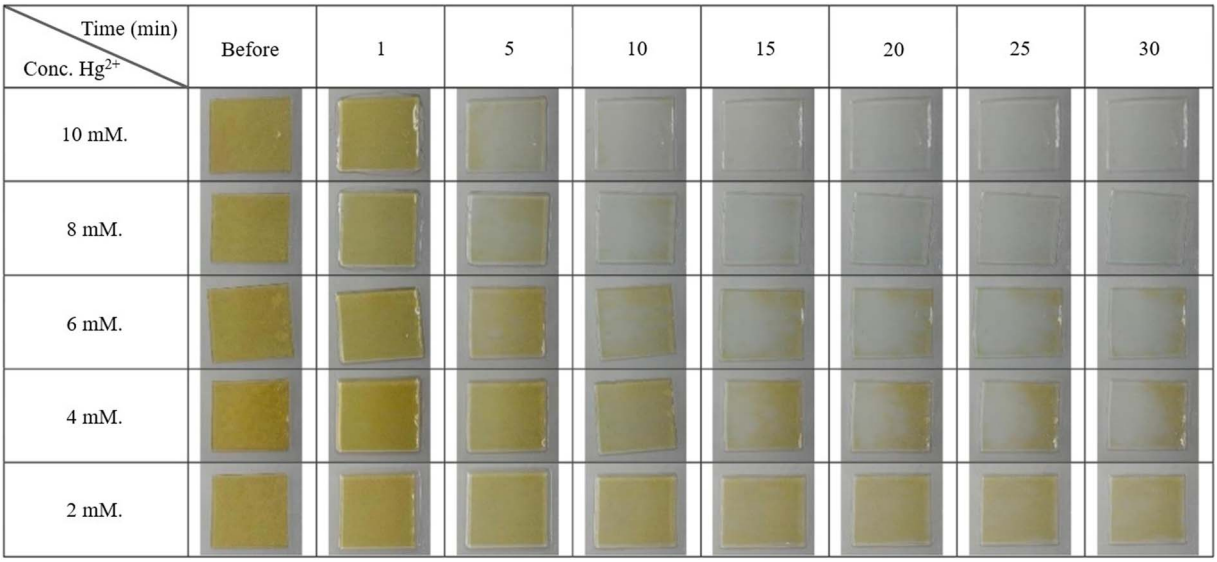

Fig. 7 The color change of the film when detecting Hg^{2+} at different concentrations.

3.5 Colorimetric sensors for Hg^{2+} detection

This study aimed to develop a sensor for detecting mercury ions using CMC-AgNPs. When mercury was dropped into the CMC-AgNPs solution, the color changed from brownish yellow to colorless. UV-vis spectroscopy analysis showed a significant decrease in the SPR absorption band of AgNPs solution containing Hg^{2+} ions, compared to the solution without Hg^{2+} ions. This demonstrates that the observed changes are specific to the interaction between mercury ions and silver nanoparticles. This can be explained by comparing the standard reduction potentials ($E°$) of Ag(I)/Ag(0) and Hg(II)/Hg(0). Since the $E°$ of Ag(I)/Ag(0) is 0.80 V, which is lower than that of Hg(II)/Hg(0) (0.85 V), Ag(0) in the AgNPs is oxidized to Ag(I),[39] resulting in an Ag–Hg amalgam. When the hydroxyl(–OH) and carboxyl(–COOH) groups of CMC interact with Hg^{2+} ions, a complex generates an Ag–Hg amalgam. The Hg^{2+} ions are quickly adsorbed onto the surface of the AgNPs, initiating an electron transfer between Ag^0 and Hg^{2+}, which leads to the formation of Ag^+ and Hg^0 ions.[40] As demonstrated in the TEM image (Fig. S2b), the formation of an Ag–Hg amalgam is observed. When AgNPs interact with mercury ions, the average particle size of AgNPs increases to 20.3 ± 4.5 nm. CMC-AgNPs have a well-functioning surface, leading to perfect aggregation and a "swelling effect", which results from the diffusion of Hg atoms, causing the overall nanoparticle size to grow.[41] Additionally, the hydrodynamic radius in the presence of mercury was examined. The results indicate that the hydrodynamic diameter of silver nanoparticles increased from 138.6 ± 7.92 nm to 163.3 ± 2.54 nm when exposed to Hg^{2+}. Moreover, the zeta potential of the silver nanoparticles rose from −26.2 ± 0.12 mV to −5.89 ± 0.82 mV. These results confirm the formation of Ag–Hg amalgam and the aggregation of AgNPs.[42]

3.6 Effect of pH for Hg^{2+} sensing

The ability to detect mercury ions using CMC-AgNPs was tested, with different pH values, as shown in Fig. 4(a) and (b), utilizing a buffer solution with a pH range between 3 and 11; acidic (HOAc buffers, pH 3.0, 4.0, 5.0 and 6.0), neutral (phosphate buffer, pH 7.0), and basic (Tris–HCl buffers (pH 8.0, 9.0, 10.0 and 11.0)). The changes can be observed from the SPR absorption band at 410 nm, calculated using the formula $A_0 - A/A_0$, where A_0 is the absorbance of the pure CMC-AgNPs, and A is the absorbance of the CMC-AgNPs after the addition of 30 μM Hg^{2+}. The result shows maximum absorbance at pH 3.0. In general, the deprotonated carboxylate group ($–COO^-$) serves as a stronger ligand than the protonated carboxyl group (–COOH). However, for Hg^{2+} ions, which are classified as soft acids under the Hard–Soft Acid–Base (HSAB) principle,[43,44] partial protonation of the carboxyl groups can enhance complex formation. The soft base nature of –COOH allows a more favorable interaction with the soft acid Hg^{2+}, promoting the formation of a stable and selective complex. Consequently, at lower pH values, moderate protonation facilitates effective coordination between Hg^{2+} ions and the CMC-AgNPs surface. Thus, pH 3 was selected as the optimal condition for all experiments.

3.7 Effect of CMC-AgNPs concentrations for Hg^{2+} sensing

The optimal concentration of CMC-AgNPs for mercury ion detection was evaluated by adding different volumes (5, 10, 30, 50, 70, 90, and 100 μL) to a 0.1 M HOAc buffer solution at pH 3.0 containing Hg^{2+}. These volumes corresponded to silver nanoparticle concentrations of 0.02, 0.05, 0.14, 0.23, 0.33, 0.42, and 0.47 nM respectively. The SPR absorption band of CMC-AgNPs at different concentrations, with both the absence and presence of Hg^{2+}, are shown in Fig. 4(c) and (d). The absorption rate ratio shows consistency across various concentrations of AgNPs. The absorbance value increases at higher concentrations, making it easier to observe changes when detecting mercury. Consequently, a CMC-AgNPs concentration of 0.47 nM (100 μL) was used for all experiments.

3.8 Effect of reaction time for Hg^{2+} sensing

This study investigated the effect of reaction time using 0.47 nM (100 μL) of CMC-AgNPs, 100 μM of Hg^{2+}, and 0.1 M HOAc buffers pH 3.0 under controlled conditions, with reaction times ranging from 1 to 10 min. The SPR absorption band was calculated using the formula $A_0 - A/A_0$, where A_0 is the absorbance of the CMC-AgNPs with Hg^{2+} at pH 3.0, and A is the absorbance of the same solution that was analyzed at times ranging from 1 to 10 min, as shown in Fig. 4(e) and (f). Following the addition of the Hg^{2+} solution, a rapid color change was observed from yellowish-brown to colorless, starting at 1 min. As shown in the scatter plot (Fig. S3) of absorbance at the maximum wavelength *versus* time, the absorbance reached its minimum at 4 min and stabilized thereafter. Consequently, the reaction time was set to 4 min for all experiments.

3.9 Selectivity studies

The selectivity of silver nanoparticles for detecting Hg^{2+} was evaluated by comparing their interactions with other transition, alkali, and alkaline earth metal ions (Na^+, K^+, Ca^{2+}, Mg^{2+}, Ba^{2+}, Mn^{2+}, Pb^{2+}, Ni^{2+}, Cd^{2+}, Cr^{2+}, Zn^{2+} and Co^{2+}). Fig. 5(a) and (b) show the UV-vis spectroscopy data. The results demonstrate no significant changes in response to other heavy metals. Furthermore, the interference was studied to examine the selective detection of Hg^{2+} by CMC-AgNPs. 100 μM of other heavy metals were added into the CMC-AgNPs solution to evaluate their effect on the sensing of Hg^{2+}. According to the results in Fig. 5(c) and (d), no significant changes were observed when other heavy metals were added together with Hg^{2+}. The naked eye experiment in Fig. 5(e) indicated that only the CMC-AgNPs solution containing Hg^{2+} exhibited a distinct color change from brownish yellow to colorless. Based on these results, it can be concluded that the CMC-AgNPs exhibit selectivity for Hg^{2+}.

3.10 Analytical performance of the optical sensor for the detection of Hg^{2+}

The mercury detection sensor by CMC-AgNPs was examined quantitively. Silver nanoparticles' absorption ratio ($A_0 - A/A_0$) was quantified at 410 nM under optimized conditions with varying Hg^{2+} concentrations. The absorption rate increased with the rising concentration of Hg^{2+} as shown in Fig. 6(a). The optical sensors using CMC-AgNPs show linear response over the 5–45 mM Hg^{2+} concentration range (Fig. 6(b)). A linear equation of $(A_0 - A/A_0) = 0.016[Hg^{2+}] - 0.0078$ was obtained with a correlation coefficient (R^2) of 0.9914. The achieved limit of detection (LOD) and limit of quantitation (LOQ) were 3.14 μM and 10.45 μM, respectively (the concentration of Hg^{2+} required to give an absorbance change ratio $(A - A_0)/A_0$ at 410 nm equal to 3 standard deviations (3σ; 10 replicate measurements of blank sample (A_0)) and 10 standard deviations (10σ) of A_0 for LOQ).

3.11 Application of CMC-AgNPs for the determination of Hg^{2+} ions in real water samples

The capability of silver nanoparticles to detect Hg^{2+} in real water samples was analyzed using UV-vis spectroscopy. The standard $HgCl_2$ (10 and 20 μM) was added to commercial drinking water. The result is depicted in Table 1. This demonstrates a strong correlation between the added and determined values, with recovery rates ranging from 99.01% to 100.65% and relative standard deviation (RSD) values between 2.58% and 1.64%.

3.12 Application of CMC-AgNPs for the determination of Hg^{2+} ions in composite films

Previous studies have demonstrated that PVA and cassava starch composite films have water-absorbing properties.[45,46] Therefore, these films were utilized as colorimetric sensors for detecting mercury ions by observing the color change of the film when exposed to mercury at different concentrations. This experiment will prepare PVA/CMC film by cutting into 1 × 1 cm per piece and dropping 200 μL of mercury solution (2, 4, 6, 8, 10 mM). The color change will be observed after 1, 5, 10, 15, 20, 25 and 30 minutes as depicted in Fig. 7. The color change from brownish yellow to colorless will be observed throughout 5 to 30 minutes. At higher Hg^{2+} concentrations, the color change occurs more distinctly.

4. Conclusions

The present study successfully extracted cellulose from *Eichhornia crassipes* (water hyacinth) and synthesized carboxymethyl cellulose (CMC) *via* the esterification method. Subsequently, silver nanoparticles (AgNPs) were synthesized using CMC as both a stabilizing and reducing agent through a physical synthesis approach. The resulting CMC-AgNPs exhibited high selectivity towards mercury (Hg^{2+}) and were employed as a colorimetric sensor for Hg^{2+} detection in both CMC-AgNPs solution and films. The presence of mercury ions induced a distinct color change from brownish yellow to colorless. The absorbance of silver nanoparticles decreased in the presence of mercury. The detection process followed a linear equation of $(A_0 - A/A_0) = 0.016[Hg^{2+}] - 0.0078$ and was obtained with a correlation coefficient (R^2) of 0.9914, with limits of detection (LOD) and quantification (LOQ) determined to be 3.14 μM and 10.45 μM, respectively and the CMC-AgNPs films detect mercury in the range from 0–10 mM in 30 min. In addition, a colorimetric sensor film was developed for Hg^{2+} detection, enhancing usability and convenience.

Author contributions

Conceptualization, S. K. and P. T., C. S., P. N.; methodology, P. T., C. S., P. N.; validation, S. K.; formal analysis, S. K., P. T., C. S., P. N.; investigation, P. T., C. S., P. N., A. S., W. O., S. Y., K. P., S. K., and S. K.; writing – original draft preparation, S. K. and P. T.; writing – review and editing, visualization, supervision, project administration, S. K. All authors have read and agreed to the published version of the manuscript.

Conflicts of interest

We wish to confirm that there are no known conflicts of interest associated with this publication.

Data availability

The datasets generated and analyzed during the current study are available within this published article and its supplementary information (SI) files. Supplementary Information is available. See DOI: https://doi.org/10.1039/d5ra04757a.

Acknowledgements

Thanks for the laboratory support from the Faculty of Science, Khon Kaen University. P. T. was financially supported by the Development and Promotion of Science and Technology Talents Project (DPST). We thank for XPS test support by Synchrotron Light Research Institute (SLRI), Thailand. This work was financially supported by the Fundamental Fund of Khon Kaen University of the year 2568 BE (FF68; Project No. 203201) with funding support from the National Science, Research, and Innovation Fund (NSRF) of Thailand.

References

1 R. A. Bernhoft, *J. Environ. Public Health*, 2012, **2012**, 460508.
2 B. Fernandes Azevedo, L. Barros Furieri, F. M. Peçanha, G. A. Wiggers, P. Frizera Vassallo, M. Ronacher Simões, J. Fiorim, P. Rossi de Batista, M. Fioresi, L. Rossoni, I. Stefanon, M. J. Alonso, M. Salaices and D. Valentim Vassallo, *J. Biomed. Biotechnol.*, 2012, **2012**, 949048.
3 X. Zhu, Y. Kusaka, K. Sato and Q. Zhang, *Environ. Health Prev. Med.*, 2000, **4**, 174–183.
4 R. M. Gardner and J. F. Nyland, *Immunotoxic Effects of Mercury*, SpringerLink, 2016, vol. 2016, pp. 231–249.
5 S. Yoon, E. W. Miller, Q. He, P. H. Do and C. J. Chang, *Angew Chem. Int. Ed. Engl.*, 2007, **46**, 6658–6661.
6 R. Shunmugam, G. J. Gabriel, C. E. Smith, K. A. Aamer and G. N. Tew, *Chem. – Eur. J.*, 2008, **14**, 3904–3907.
7 S. K. Kim, H. J. Lee and J. H. Park, *Sens. Actuators B: Chem.*, 2018, **261**, 201–215.
8 S. Patel, *Rev. Environ. Sci. Biotechnol.*, 2012, **11**, 249–259.
9 T. Chaiwarit, B. Chanabodeechalermrung, N. Kantrong, C. Chittasupho and P. Jantrawut, *Gels*, 2022, **8**, 767.
10 S. M. M. Shanab, E. A. Shalaby, D. A. Lightfoot and H. A. El-Shemy, *PLoS One*, 2010, **5**, e13200.
11 A. J. Hargreaves, P. Vale, J. Whelan, C. Constantino, G. Dotro and E. Cartmell, *Water, Air, Soil Pollut.*, 2016, **227**, 89.
12 M. M. Al-Sulaiti, L. Soubra and M. A. Al-Ghouti, *Curr. Pollut. Rep.*, 2022, **8**, 249–272.
13 T. Istirokhatun, N. Rokhati, R. Rachmawaty, M. Meriyani, S. Priyanto and H. Susanto, *Procedia Environ. Sci.*, 2015, **23**, 274–281.
14 A. H. Saputra and R. A. Purwoko, *AIP Conf. Proc.*, 2018, **2024**, 020029.
15 M. S. Yeasmin and Md. I. H. Mondal, *Int. J. Biol. Macromol.*, 2015, **80**, 725–731.
16 R. L. Feddersen and S. N. Thorp, in *Industrial Gums*, ed. R. L. Whistler and J. N. Bemiller, Academic Press, London, 3rd edn, 1993, pp. 537–578.
17 F. He and D. Zhao, *Environ. Sci. Technol.*, 2007, **41**, 6216–6221.
18 A. K. S. Rawat, K. Balakrishnan and S. K. Shukla, *Environ. Sci. Technol.*, 2013, **47**, 123–134.
19 T. Bruna, F. Maldonado-Bravo, P. Jara and N. Caro, *Int. J. Mol. Sci.*, 2021, **22**, 7202.
20 K. Plaeyao, R. Kampangta, Y. Korkokklang, C. Talodthaisong, A. Saenchoopa, S. Thammawithan, K. Latpala, R. Patramanon, N. Kayunkid and S. Kulchat, *RSC Adv.*, 2023, **13**, 19789–19802.
21 X.-F. Zhang, Z.-G. Liu, W. Shen and S. Gurunathan, *Int. J. Mol. Sci.*, 2016, **17**, 1534.
22 J. Y. Cheon and W. H. Park, *Int. J. Mol. Sci.*, 2016, **17**, 2006.
23 A. Aravind, M. Sebastian and B. Mathew, *New J. Chem.*, 2018, **42**, 15022–15031.
24 A. Saenchoopa, W. Boonta, C. Talodthaisong, O. Srichaiyapol, R. Patramanon and S. Kulchat, *Spectrochim. Acta, Part A*, 2021, **251**, 119433.
25 J. Y. Song and B. S. Kim, *Bioprocess Biosyst. Eng.*, 2009, **32**, 79–84.
26 D. Sasikala, K. Govindaraju, S. Tamilselvan and G. Singaravelu, *Biotechnol. Bioproc. E*, 2012, **17**, 1176–1181.
27 N. Abdel-Raouf, N. M. Al-Enazi, I. B. M. Ibraheem, R. M. Alharbi and M. M. Alkhulaifi, *Saudi J. Biol. Sci.*, 2019, **26**, 1207–1215.
28 D. K. Verma, S. H. Hasan and R. M. Banik, *J. Photochem. Photobiol., B*, 2016, **155**, 51–59.
29 K. Logaranjan, A. J. Raiza, S. C. B. Gopinath, Y. Chen and K. Pandian, *Nanoscale Res. Lett.*, 2016, **11**, 520.
30 A. A. Hebeish, M. H. El-Rafie, F. A. Abdel-Mohdy, E. S. Abdel-Halim and H. E. Emam, *Carbohydr. Polym.*, 2010, **82**, 933–941.
31 J. S. Yaradoddi, N. R. Banapurmath, S. V. Ganachari, M. E. M. Soudagar, N. M. Mubarak, S. Hallad, S. Hugar and H. Fayaz, *Sci. Rep.*, 2020, **10**, 21960.
32 M. M. Mazlan, L. K. Kian, H. Fouad, M. Jawaid, Z. Karim and N. Saba, *Biomass Conv. Bioref.*, 2024, **14**, 14653–14663.
33 D. S. Lakshmi, N. Trivedi and C. R. K. Reddy, *Carbohydr. Polym.*, 2017, **157**, 1604–1610.
34 Z. N. T. Mzimela, L. Z. Linganiso, N. Revaprasadu and T. E. Motaung, *Mater. Res.*, 2018, **21**, e20170750.
35 A. H. Naeini, M. R. Kalaee, O. Moradi, R. Khajavi and M. Abdouss, *Adv. Compos. Hybrid Mater.*, 2022, **5**, 335–349.
36 H. Hantsche, *Adv. Mater.*, 1993, **5**, 778.
37 J. Liu, D. A. Sonshine, S. Shervani and R. H. Hurt, *ACS Nano*, 2010, **4**, 6903–6913.
38 V. K. Sharma, R. A. Yngard and Y. Lin, *Adv. Colloid Interface Sci.*, 2009, **145**, 83–96.
39 Y. Thepchuay, N. Jommala, T. Wonglakhon, P. Nuengmatcha, B. Ninwong, N. Saengsane, P. Sricharoen and N. Limchoowong, *Arab. J. Sci. Eng.*, 2023, **48**, 7825–7839.
40 S. Y. Sharaf Zeebaree, O. I. Haji, A. Y. S. Zeebaree, D. A. Hussein and E. H. Hanna, *Catalysts*, 2022, **12**, 1464.
41 A. Abbasi, S. Hanif and M. Shakir, *RSC Adv.*, 2020, **10**, 3137–3144.

42 S. Balasurya, A. Syed, A. M. Thomas, N. Marraiki, A. M. Elgorban, L. L. Raju, A. Das and S. S. Khan, *Spectrochim. Acta, Part A*, 2020, **228**, 117712.
43 R. G. Pearson, *J. Chem. Educ.*, 1968, **45**, 581.
44 Y. Zhou, J. Zhang, X. Luo and Y. Luo, *BioResources*, 2016, **11**, 7145–7161.
45 Y. Song, S. Zhang, J. Kang, J. Chen and Y. Cao, *RSC Adv.*, 2021, **11**, 28785–28796.
46 J. Arayaphan, P. Boonsuk and S. Chantarak, *Iran. Polym. J.*, 2020, **29**, 749–757.